Journal of Inorganic and Organometallic Polymers and Materials
https://doi.org/10.1007/s10904-024-03212-2

RESEARCH

Green Synthesis of Silver Nanoparticles Using Chitosan in Carbonic acid Solutions: Effect of Pressure and Temperature on the Structure and Antimicrobial Properties

Ivan S. Chaschin[1] · Evgenii I. Perepelkin[1] · Eduard E. Levin[2] · Sergey S. Abramchuk[1] · Nelya M. Anuchina[3] · Olga A. Kizas[1] · Yulia V. Ryzhova[1] · Natalia P. Bakuleva[3]

Received: 23 April 2024 / Accepted: 11 June 2024

Abstract
Composite chitosan films containing stabilized silver nanoparticles were synthesized using aqueous solutions of carbonic acid (i.e., water saturated with carbon dioxide) under varying pressure (6–50 MPa) and temperature conditions (25–90 °C). Carbonic acid is a biocompatible and antimicrobial medium. The influence of various factors, such as the molar ratio of chitosan to silver, pressure variations, and temperature, on the structural properties of the composite chitosan/silver composites was studied systematically using transmission electron microscopy (TEM) and X-ray diffractometry (XRD). A correlation was identified between the characteristics of the water saturation with carbon dioxide (pressure and temperature of the carbonic acid solution) and the structural features of the composite films. All films exhibited small silver nanoparticles measuring 1–2 nm in diameter. At specific pressure and temperature values, a phase of larger nanoparticles with sizes in the tens of nanometers was also present within the chitosan matrix. The relationship between the structure of the produced films and their antimicrobial properties has been established.

Keywords Chitosan · Silver nanoparticles · Carbonic acid · High pressure · Antimicrobial properties

1 Introduction

Chitosan is a polysaccharide characterized by a randomly distributed β-(1→4)-linked D-glucosamine and N-acetyl-D-glucosamine monomers, with a wide range of molecular weights (MW), degree (DA) and pattern (PA) of N-acetylation [1]. This polymer is obtained from alkaline hydrolysis of chitin, which is the second of the most abundant natural amino polysaccharide extracted from the exoskeleton of crustaceans and insect, from fungal cell walls, etc [2–4]. Chitosan has excellent biological properties, including being nontoxic, mucoadhesive, hemocompatible, biodegradable, and possessing antitumor, antioxidant, and antimicrobial properties [5–10]. These properties make chitosan a

✉ Ivan S. Chaschin
chaschin@polly.phys.msu.ru

Evgenii I. Perepelkin
perepelkinj@mail.ru

Eduard E. Levin
levin@elch.chem.msu.ru

Sergey S. Abramchuk
abr@polly.phys.msu.ru

Nelya M. Anuchina
anuchinanelya@mail.ru

Olga A. Kizas
kizas@ineos.ac.ru

Yulia V. Ryzhova
ryzhova.iuv@phystech.edu

Natalia P. Bakuleva
npbakuleva@yandex.ru

[1] Nesmeyanov Institute of Organoelement Compounds, Russian Academy of Sciences, Vavilova 28, Moscow 119991, Russian Federation

[2] Faculty of Chemistry, Lomonosov Moscow State University, Leninskie gory 1–2, Moscow 119991, Russian Federation

[3] Bakulev Scientific Center for Cardiovascular Surgery, Rublevskoe Sh. 135, Moscow 121552, Russian Federation

Published online: 07 October 2024

very attractive biomaterial for different applications in the biomedical field.

Despite the fact that the first studies on the antimicrobial activity of chitosan were published four decades ago [11, 12], scientific interest in this property has never waned, and to this day, as evidenced by the thousands of publications published in the last few years alone. In addition, interest in the antibacterial properties of chitosan is associated with nanotechnologies leading to the development of several mixed nanosystems (for example, nanoparticles, nanocomposites) in which chitosan is coordinated with metals or plays the role of a carrier for natural or synthetic compounds with internal antibacterial activity [13–15].

The combined antimicrobial effect of chitosan and metals was discovered to obtain new nanocomposite materials with improved microbicides properties [16, 17]. In particular, a wide range of actions against both Grampositive and Gram-negative bacteria have been established for gold, silver or copper nanoparticles loaded in chitosan matrix [15, 18–20]. Such nanoparticles were prepared by adding metal ion solutions to the nanosuspension of chitosan, or by reducing the soluble metal salt in the presence of chitosan solutions [21].

Silver-based nanocomposites are the most frequently explored chitosan complexes with metals [22–24]. Bruna et al. discussed silver nanoparticles (AgNPs) activity and mechanisms of action against *Staphylococcus aureus* and *Escherichia coli*. They demonstrated that silver nanoparticles have higher antibacterial effect than silver ions. The maximum antibacterial effect was observed at a concentration close of that of the electrical percolation threshold [25]. The increased antimicrobial activity of AgNPs can be explained by the fact that smaller silver nanoparticles have a higher specific surface area and release Ag^+ ions at a faster rate [26].

Macromolecules of chitosan are able to coordinate silver ions thanks to the presence of a large number of amino groups in the polymer chain. Therefore, chitosan has the ability to stabilize the AgNPs. It has been shown that it is possible to form metallic AgNPs in a chitosan solution [27]. Later it was found that chitosan also plays the role of silver reducing agent [28].

In all these studies, the solutions of acetic acid were used as a solvent for chitosan. Acetic acid is not absolutely biocompatible solvent. Acetic acid serves in a human body as a promoter of the allergenic reaction presumably by a hapten mechanism [29–31].

However, there is a different solvent chitosan — carbonic acid. Carbonic acid is a promising solvent of chitosan in terms of biomedical applications. First, this solvent has antimicrobial properties. Carbonic acid solutions under the pressure of water saturating CO_2 demonstrate certain antimicrobial properties since dissolved CO_2 molecules penetrate into the bacteria, viruses, or spores dispersed in the aqueous phase and biologically inactivate them [32–34]. Secondly, after decompression, carbonic acid spontaneously breaks down to absolutely safe for the human body components: water and CO_2. Thus, the problem of residual solvent in the product is automatically solved, even such a relatively harmless one as acetic acid. Third, it is possible to change the pH instantly and isotropically throughout the volume by a simple pressure variation. Since chitosan is a pH-dependent polymer, the pressure variation can change the solubility of carbonic acid with respect to chitosan. Sakai, Hayano, Yoshioka, and Yoshioka (2001) [35] first proposed to dissolve chitosan in water bubbled with CO_2. Later, Otake et al. (2006) [36] studied the chitosan solubility in carbonic acid solutions at moderate pressure of 8 MPa. Recently, we were successfully worked methodology modification of collagen matrices for biological prosthetic heart valves, with solutions of carbonic acid [37, 38]. It was shown that exposure of the bovine pericardium in solutions of chitosan in aqueous carbonic acid leads to highly pronounced antimicrobial activity against biofilm formation of relevant Gram-positive and Gram-negative strains [37]. Moreover, it was shown that the pressure variation can be controlled by adsorption of chitosan on collagen tissue [39]. Thus, solutions of carbonic acid are very promising for applying in medicine in general when acidity is required and could be used instead of solutions of acetic acid (or any other acid) in biomedical applications related to chitosan.

We have tested a fundamentally different approach to the production of composite chitosan films with Ag NPs using instead of classical solvents chitosan water saturated with CO_2 under pressure (carbonic acid). It was found that it is possible to control the structure of composite chitosan films obtained from chitosan solutions with silver nitrate by varying the solvent capacity of carbonic acid. Was investigated two strategies changes the dissolving ability of carbonic acid: by adding small quantities of acetic acid, as well as pressure changes in solution. It was found that improving of the quality of the solvent by adding acetic acid decrease the size of large silver nanoparticles, which is most likely due to the expansion of the chitosan macromolecule, which increase the stabilizing ability of the polymer [40]. With increasing pressure in carbonic acid from 6 to 35 MPa, the transition of the chitosan film from the structure with the phase with small Ag NPs (1–2 nm) to the structure with bimodal size distribution of nanoparticles occurs, where, along with small particles, a phase of crystalline large Ag NPs (40–50 nm) is formed [41]. It is worth noting that low concentrations of the silver precursor were studied in these works and the chitosan/Ag composites were only obtained in the form of dried thin films. Also, it is noteworthy that the recovery of silver ions in solutions was only due to

chitosan chains. However, Novikov et al. (2018) found that the higher degree of Ag nanoparticles reduction could be achieved with using self-eliminating gaseous hydrogen as a reducing agent that may be easily admixed to carbon dioxide in the reactor [42]. Such a usage of hydrogen is beneficial as far as it allows to minimize chitosan participation in redox processes thus preserving its biocompatibility. In this study, carbon dioxide solutions were used to create chitosan-metal nanocomposites. The authors focused on obtaining the composites at room temperature and under a fixed pressure of 30 MPa, but they did not explore other conditions or parameters.

In many articles the attention is focused on the fact that chitosan can restore the ions to Ag metal in acetic acid solutions only at elevated temperature (approximately 80 °C). This feature can be explained by the weak oxidizing properties of silver ions and the weak reducing ability of chitosan [43]. Therefore, at relatively low temperatures the reduction reaction is very slow. On the other hand, elevated temperatures lead to enhanced aggregation of silver nanoparticles. Because, a key feature of this medium is the possibility to control the pH, and, therefore, it stability to dissolve the polymer by changing pressure and temperature and that chitosan chains in carbonic acid take a special compact conformation [44], the temperature and pressure effect on the structure of films obtained from solutions in carbonic acid may differ significantly from the studied cases with the use of acetic acid in which the macromolecules of chitosan have the conformation of straightened conformation.

In this study, we systematically investigate the impact of various factors on chitosan-based composite films containing Ag NPs. These factors include the molar ratio of chitosan to silver, pressure, and temperature. We use chitosan composite films loaded with Ag NPs as models for simulating the formation of nanoparticles in gels and solutions under pressure and temperature conditions. A significant aspect of our work is that we only use chitosan as a reducing and stabilizing agent for metal particles. This approach allows us to precisely control the influence of each variable parameter on the composite film structure. Additionally, we expect to reveal the relationship between the composite's structure and its antimicrobial properties for the first time.

2 Experimental

2.1 Materials and Experimental Setup

In our work, we used chitosan sample (low molecular chitosan #448,869) silver nitrate (99.9999% trace metal basis) #204,390, all supplied by Sigma-Aldrich. The molecular weight of chitosan samples was measured by gel permeation chromatography and viscosimetry, whereas the degree of deacetylation was determined by pH titration and IR spectroscopy (for low molecular chitosan #448,869: Mw_{chit}=210 kg/mol, Mn_{chit}=77 kg/mol, $M\eta_{chit}$ = 80 kg/mol, DD = 84%). Water used in the experiments was purified on a Millipore Milli-Q Synthesis equipment and was prepared just before each experiment. In the present research we employed CO_2 of high purity (> 99.995%, Moscow Gas Refinery Plant, Russian Federation) to saturate water and thus generate carbonic acid solution.

The experimental setup [37, 40] was engineered for the dissolution of chitosan in carbonic acid solutions. The setup consists of a piston pressure generator with electronic control (Thar, USA), a mechanical manometer, a cylinder with carbon dioxide, and a home-made 30-ml high-pressure stainless steel reactor with brass jacket capable to withstand the pressure up to 70 MPa (autoclave-cuvette). All the components of the experimental setup are interconnected by the system of capillaries and valves.

2.2 Synthesis of Composite Chitosan-Based Films with Ag Nanoparticles in Solution of Carbonic Acid. Preparation of Samples for Different Methods of Research

2.2.1 Dissolution of Chitosan in Aqueous Solution of Carbonic acid and Subsequent Composite Solutions Formation

Synthesis of AgNPs in solutions of chitosan in aqueous carbonic acid was carried out as follows. A sample of m = 150 mg of the chitosan material was placed into the autoclave. Then 15 ml of freshly prepared Milli-Q water was added into an autoclave. An autoclave with chitosan sample and water was then immersed in a thermostat at 25 °C and CO_2 pumped to a fixed pressure which varied from 6 to 50 MPa and chitosan was dissolved on a magnetic stirrer for a week to achieve homogeneous dissolution of chitosan in carbonic acid. After that, the reactor was slowly decompressed (the decompression rate averaged 2.0 MPa per minute). It was found that after the week exposure, the obtained solution was clear. Therefore, complete solubility of chitosan in aqueous solution of carbonic acid after the week exposure at room temperature is achieved for these concentrations. Next, a solution of silver nitrate in water was prepared. For that, a certain amount (depending on the desired ratio of moles of silver atoms to moles of chitosan monomer units) of crystalline $AgNO_3$ was dissolved in 300 µl of freshly prepared Milli-Q water and then the obtained silver salt solution was added to the previously prepared (see above) solution of chitosan in aqueous carbonic acid. In our study, we investigated two different ratios of the precursor

to chitosan – 5 units of chitosan per silver ion (concentration $AgNO_3$ — 13.5 mM/l, chitosan concentration — 1.0 weight%) and 15 units of chitosan per silver ion (concentration $AgNO_3$ — 4.5 mM/l, chitosan concentration — 1.0 weight%). The pressure in the reactor was again raised up to up to selected pressure value (in the range of 6 to 50 MPa, the same as in the preparation of the chitosan solution). The temperature effect was investigated under conditions of constant pressure (P_{CO2}=35 MPa) and exposure time. The reactor was injected with CO_2 at room temperature to a pressure that at a given temperature in the thermostat will be set to a value of 35 MPa. The calculation of the desired pressure was determined according to NIST Chemistry WebBook, SRD 69. The exposure was carried out for *8 h* at the temperature variations: 50 °C, 65 °C, 80 °C, 90 °C. To study the light scattering of solutions obtained from temperature variations (50°C, 80°C, and 95 °C), a polymer solution with a low concentration (c = 0.5 g/l) and a precursor solution with a concentration of 0.25 mM/l were prepared.

2.2.2 Preparation of Samples for TEM Study

To investigate the chitosan-stabilized nanoparticles with TEM, the obtained gels were dried at a constant temperature 25° in a dark place. In such a drying procedure, the gels collapsed into condensed-phase films. Thin cuts were made from the resulting films using an Ultracut ultramicrotome (Reichert-Jung, Austria) with a diamond knife ultra 35° (DiaTOME, Switzerland). The cuts were transferred directly from the surface of the knife using dry method (i.e., not from the surface of water because the cuts were wetted by water) to a carbon substrate film (S160, Plano GmbH, Germany) fixed on a copper grid.

2.3 Experimental Methods of Research

2.3.1 Studies by TEM

Thin cuts obtained with an ultramicrotome were studied by transmission electron microscopy. TEM micrographs were obtained on a LEO 912 AB OMEGA microscope (LEO/Carl Zeiss, Germany) at an accelerating voltage of 100 kV.

2.3.2 UV-VIS Spectroscopy

The UV-VIS spectra of chitosan solutions with synthesized Ag NP in carbonic acid was measured using a Helios Alpha spectrophotometer (Thermo Scientific, USA) in a quartz cell (wavelength ranging from 190 to 1100 nm in 1 nm increments). Before the experiment, 1 ml of each chitosan with silver nanoparticles sample was dissolved in 2 ml of 1% aqueous solution of acetic acid. The spectrum of 1% aqueous acetic acid was used as a baseline.

2.3.3 Dynamic Light Scatter (DLS) Analysis of the Chitosan/AgNPs Solutions

The light scattering of weakly concentrated chitosan solutions with silver nanoparticles obtained under temperature variation (p.2.2.1) was investigated. The study was carried out with the particle analyzer Malvern Zeta-Sizer Ultra (Malvern Instruments Ltd., UK) by the dynamic light scattering method. Relaxation time distribution functions and hydrodynamic radii were calculated using the analysis package CONTIN data. All the dynamic light scattering experiments were held under scattering angles from 40 to 150°.

2.3.4 X-ray Diffraction Analysis

X-ray diffraction patterns were collected on a Rigaku D/max-RC Xray diffractometer in a step scan mode (CuKα-radiation, a graphite crystal diffracted beam analyzer, a scintillation detector) in the Bragg-Brentano geometry. To increase signal to background ratio, the specimens were mounted on a zero-background holder with a sapphire crystal [45]. Phase identification was done with ICDD PDF2 database (http://www.icdd.com/products/pdf2.htm, 2017).

2.3.5 Antimicrobial Tests

Antimicrobial tests of composite chitosan films of different structure, obtained from solutions at variation of pressure and temperature values, were carried out. Tests were performed in accordance with GOST R ISO 11737-1-2012. Antimicrobial activity was assessed by zone of lysis around the film samples of $\sim 1 \times 1$ cm^2, placed on a dense nutrient medium seeded with a lawn of the Museum strains of test-cultures — *Staphylococcus aureus ATCC 29,213, Escherichia coli ATCC 25,922, Pseudomonas aeruginosa ATCC 27,853, Enterococcus faecalis ATCC 29,213 and spore-forming culture of Bacillus subtilis ATCC*, taken at a concentration of 10^6 cell/ml (according to McFarland with the use of the instrument Densi-La-Meter, of the company bio Merieux, France). As a control, a film of chitosan without silver nanoparticles was taken. The antimicrobial activity index was estimated from the ratio: $I = 1 - \frac{D_o}{D_c}\%$, where I is the index of antimicrobial activity, D_0 — is the diameter of the bacterial growth zone for samples of composite chitosan films, D_c — is the diameter of the bacterial growth zone for the control chitosan film [46].

3 Results and Discussion

In this paper we systematically investigated the effect of pressure (P) and temperature (T) of chitosan solutions in carbonic acid on the structure of composite chitosan films obtained from this solution. At the same time, two types of films with different precursor concentrations were obtained: 1 silver ion at 15 chitosan links and 1 silver ion at 5 chitosan links.

We revealed that when $AgNO_3$ salt is added to chitosan dissolved in carbonic acid solutions, chitosan gels are formed. To study the regularities of the formation of silver nanoparticles, films were obtained as a result of drying and collapse of such gels.

Based on the results of TEM, it was detected that small silver nanoparticles are present in large amounts in all the samples. It was found that depending on the parameters of pressure and temperature in the solution is possible the formation of two types of structures in the film: (1) one modal distribution of small metallic silver nanoparticles (2–5 nm), (2) bimodal distribution of particle size along with the phase of small particles is present and the phase of large nanoparticles (10–100 nm). Note that in Fig. 1 and the following figures, images of sections of composite samples are presented at different scales. This allows us to prove the presence of a typical and non-random structure for a particular type of sample. In addition, the figures show diffraction patterns from crystallites that are localized over a sufficiently large area of the samples. This can be considered as a kind of integrated structural assessment. Films with small particles are characterized by continuous bands of diffraction rings (Fig. 1d, e). The film obtained from the solution under the highest pressure ($P = 35$ MPa), on the other hand, has pronounced dots in its diffraction pattern, indicating the presence of larger crystallites (Fig. f). In both cases, diffraction patterns provide information about the structure of the sample.

No significant influence of precursor concentration on the structure of composite films was revealed. They are uniformly distributed in the gel, and their average size is around 2–5 nm (these nanoparticles look like dark spots in the TEM micrographs, see Figs. 1 and 2). However, some films obtained under certain conditions are characterized by the presence of a second type of structure with the presence of large nanoparticles. Indeed, it was found that in solutions of carbonic acid at a pressure of 6 MPa and 35 MPa, large nanoparticles are formed with a low precursor concentration. It is noteworthy that large nanoparticles and agglomerates of them are formed at a high concentration of the precursor at 6 MPa and 50 MPa. No matter the precursor concentration at an intermediate pressure of 20 MPa, the formation of large nanoparticles. It is worth noting the influence of precursor concentration on the structure of the obtained films. With increasing precursor concentration at high pressure, large silver nanoparticles and their agglomerates are formed (Figs. 1 and 2).

To determine the phase composition of films dried from gels, X-ray diffraction (XRD) was used. On the figure, straight lines corresponding to the tabulated positions of the metallic silver peaks (card #4-0783, http://www.icdd.com/products/pdf2.htm, 2017). Diffraction spectra of films obtained by watering from solutions in carbonic acid at different pressures and temperatures indicate the presence of metallic silver for all samples. In addition, there are peaks

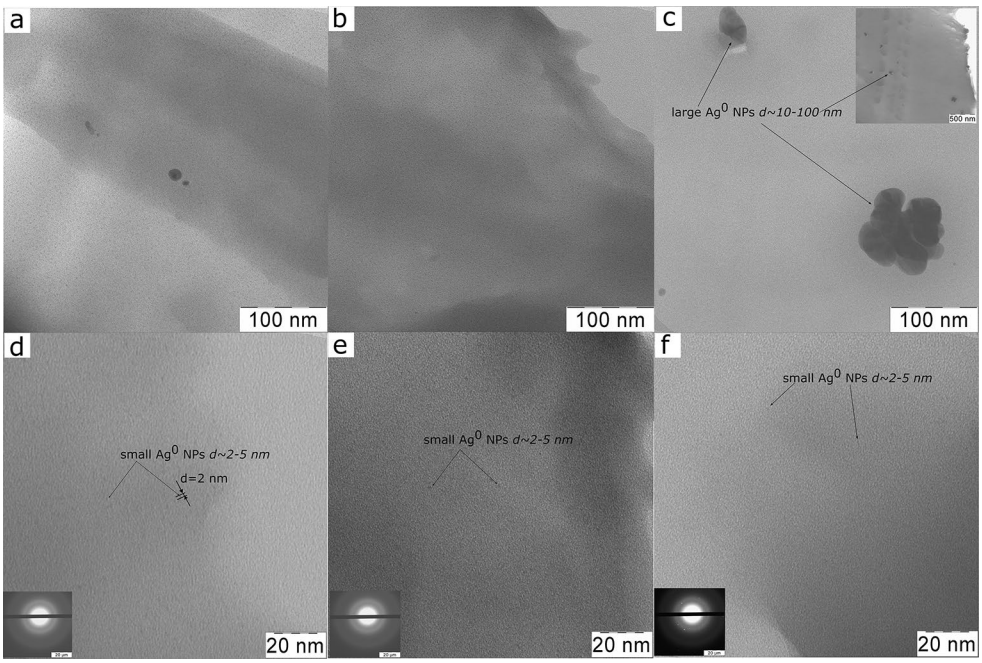

Fig. 1 TEM image of ultrathin sections of the composite chitosan films with Ag NPs obtained with irrigation from 1% weight chitosan solution (T = 25 °C, $AgNO_3$ concentration — 4.5 mM/l, exposure for 8 h at different pressures: (**a**, **d**) – 6 MPa, (**b**, **e**) – 20 MPa, (**c**, **f**)– 35 MPa. Top row - magnification ×300k (scale line – 100 nm), bottom row - ×1000k (scale line – 20 nm). In the upper right corner of the (**c**) image, there is a image of the same sample presented on a larger scale (×40k). Diffraction patterns for composite films are shown in the lower left corner of the lower row images

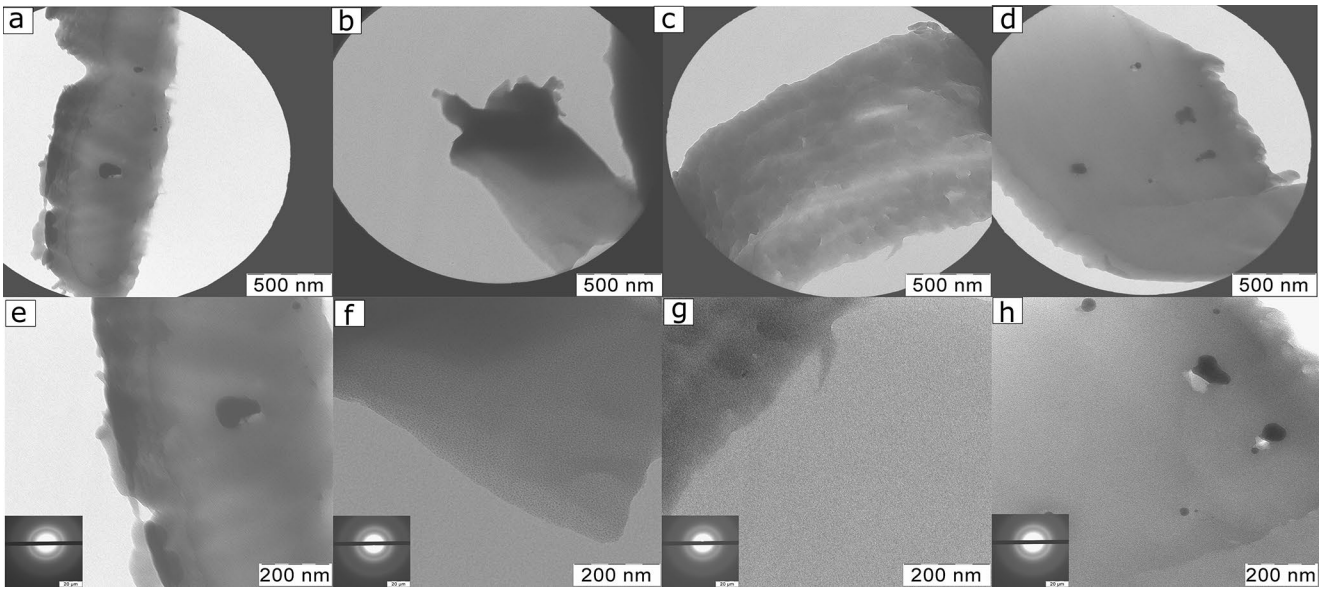

Fig. 2 TEM image of ultrathin sections of the composite chitosan films with Ag NPs obtained with irrigation from 1% weight. chitosan solution (T = 25 °C MPa, concentration $AgNO_3$ — 13.5 mM/l, exposure for 8 h at different pressures: (**a**, **e**) – 6 MPa, (**b**, **f**) – 20 MPa, (**c**, **g** – 35 MPa, (**d**, **h**) – 50 MPa. Top row - magnification ×40k (scale line – 500 nm), bottom row - ×100k (scale line – 200 nm). Diffraction patterns for composite films are shown in the lower left corner of the lower row images

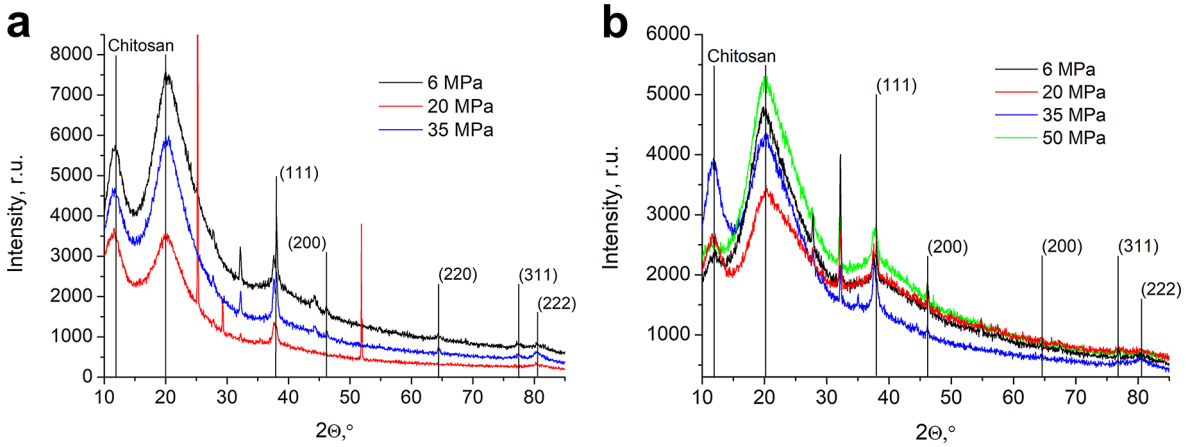

Fig. 3 X-ray diffraction patterns of chitosan nanocomposite films with silver nanoparticles prepared by irrigation from chitosan solutions with an $AgNO_3$ precursor in a solution of carbonic acid at different pressures, at a polymer concentration of cite = 10 g/l and at room temperature: (**a**) precursor concentrations - ν Ag = 4.5 mM/l (1 Ag ion per 15 units of chitosan), (**b**) precursor concentrations – ν Ag = 13.5 mM/l (5 Ag ions per 15 units of chitosan)

of chitosan — two broad reflexes at 11.6 and 20.3 º [47]. Diffraction spectra of films obtained from the solution at a pressure of 6 MPa and 35 MPa at low precursor concentration and at 6 MPa, 50 MPa at high precursor concentration have reflexes (111), (222), (200) and (220), which suggests that the nanoparticles in this film have a spherical shape, in contrast to the expected shape of nanoparticles in other samples, which, based on the below diffraction spectra (Fig. 3), which should have an asymmetric non-spherical shape. In addition, based on the obtained diffraction spectra, it follows that the amount of the crystalline phase of silver in films obtained from solutions at pressures of 20 MPa is significantly less than for films obtained at high pressure, which is confirmed by the results of analysis of their structure using TEM [41].

By the width of the radiograph peaks at half-height, it is possible to determine the size of the nanocrystal region, according to the Debye-Scherrer formula [48]:

$$B = \frac{\lambda}{\Delta\theta * Cos\theta} \quad (1)$$

Where B — is the size of nanocrystals, $\Delta\theta$ — is the width of the peak at half-height, λ — is the wavelength of x-rays.

Table 1 The size of metallic silver nanocrystals, the size of nanoparticles of nanoparticles in composite chitosan films obtained from chitosan solutions in carbonic acid at different pressures (T = 25 °C, $AgNO_3$ concentration — 4.5 mM/l, exposure for 8 h). The crystallite size is calculated using the full width at half maximum (FWHM) of the (111) reflection, as determined by the Debye-Scherrer equation, for all sample types in Fig. 3

Pressure, MPa	Size of Ag nanocrystals, nm	Size of AgNPs, nm
6	3.0 ± 1.0	1.5 ± 0.5
20	3.0 ± 1.0	1.5 ± 0.5
35	10.0 ± 2.0	9.0 ± 1.0

The sizes of metal silver nanocrystals in chitosan films were determined using the obtained x-ray diffraction patterns of nanocomposite chitosan films according to the Debye-Scherrer formula. It was found that the size of silver nanocrystals depends on the pressure (Table 1). The size of silver nanocrystals for films obtained from solutions at 35 MPa corresponds to the size of individual nanoparticles of this sample, previously measured using TEM. For other samples, the size of nanocrystals was twice the size of nanoparticles, which is somewhat strange. However, it must be taken into account that the RDA is a method that provides an integral estimate for the entire sample, whereas the TEM is a local method for studying the structure. Apparently, based on the intensity of the peaks and the results of TEM, metallic silver nanocrystals in films obtained from solutions at pressures of 6 and 30 MPa are present in a very small amount.

To study the temperature effects, we selected an intermediate pressure value in the water/carbon dioxide system, where there is sufficient acidity in the aqueous phase to allow chitosan to dissolve over a wide range of temperatures [49]. For films obtained by variation of the temperature of the XRD showed the presence of characteristic peaks of chitosan — two convenient reflexes in 11.6 and 20.3 º 2θ. In addition, expanded silver with two orders of reflection (111) was found in all samples. Reflexes at 2θ = 37.57 and 80.56 º, respectively, the first and second order of reflection (111) with periods d = 2.39 and 1.19 Å (Fig. 3). In normal silver, these values are 2.359 And 1.179 a, respectively. For a sample of a composite film obtained from a solution at a temperature of 95 °C, in addition to the peaks of chitosan and expanded silver, the presence of polycrystalline metallic silver is characteristic.

For films obtained by varying the temperature, the XRD also showed the presence of characteristic chitosan peaks — two broad reflexes at 11.6 and 20.3º 2θ. In addition, expanded silver with two orders of reflection (111) was detected in all samples. Reflexes at 2θ = 37.57 and 80.56º, respectively, the first and second order of reflection (111) with periods d = 2.39 and 1.19 Å (Fig. 4). In normal silver, these values are 2.359 and 1.179 Å, respectively. For a sample of a composite film obtained from a solution that was at a temperature of 95 °C in addition to the peaks of chitosan and expanded silver the presence of polycrystalline metallic silver is characteristic.

The analysis of the UV-vis spectra of chitosan solutions containing silver precursor, after exposure at various temperatures for a fixed exposure time of 8 h, revealed the presence of a surface plasmon resonance peak [50] at a wavelength of 420 nm at a temperature of 95 °C (Fig. 5). The presence of a pronounced peak of the solution correlates with the picture of X-ray diffraction analysis, where the peaks of crystal silver are clearly visible. Most likely, the integral pattern of both the solution and the composite film obtained from the solution indicates the presence of large metallic particles in such a system after exposure at high temperature.

Indeed, by analyzing TEM images and electron diffraction of the composite film samples (Figs. 6 and 7), it was found that metallic silver nanoparticles are present in the films. Indeed, both in the insets in Fig. 6 and in the insets

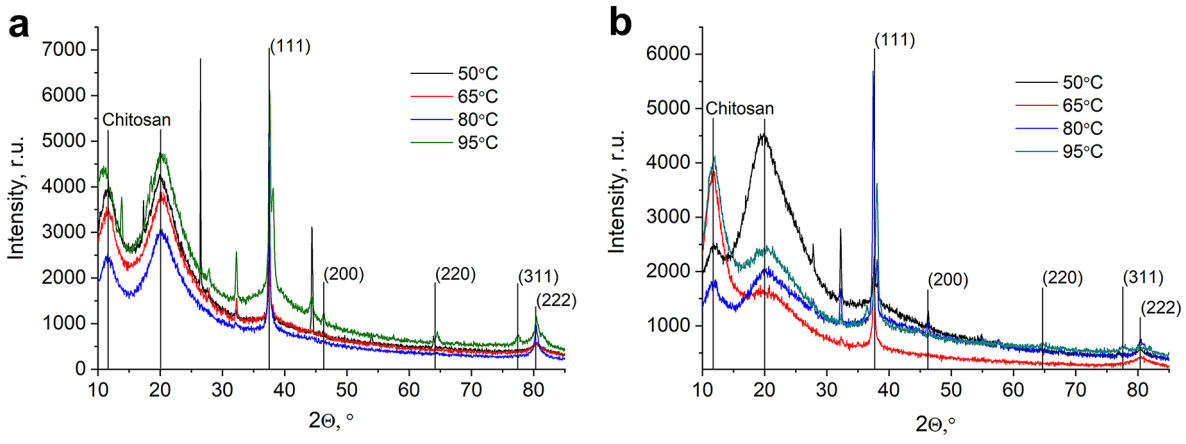

Fig. 4 X-ray diffraction patterns of chitosan nanocomposite films with silver nanoparticles prepared by irrigation from chitosan solutions with an $AgNO_3$ precursor in a solution of carbonic acid at different values of temperature, at a polymer concentration of cite = 10 g/l and at pressure of 350 atm : (**a**) precursor concentrations - ν Ag = 4.5 mM/l (1 Ag ion per 15 units of chitosan), (**b**) precursor concentrations - ν_{Ag} = 13.5 mM/l (5 Ag ions per 15 units of chitosan)

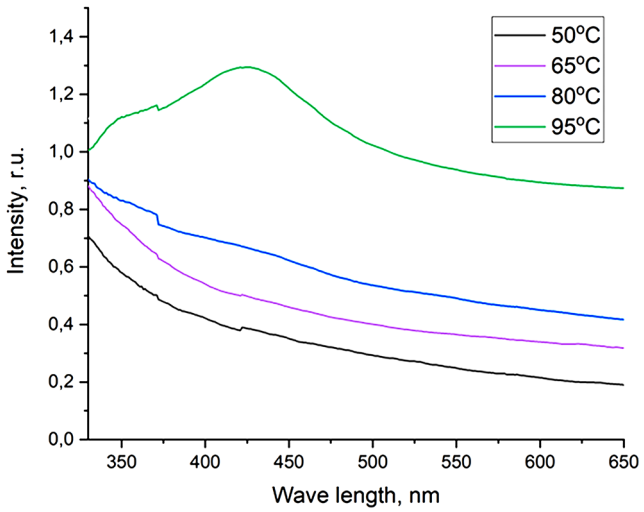

Fig. 5 UV-vis spectra 1% weight. chitosan solution ($P = 35$ MPa, precursor $AgNO_3$ concentration — 13.5 mM/l, exposure for 8 h at different temperatures: 50 °C; 65 °C; 80 °C; 95 °C

in Fig. 7, the radii of the diffraction rings are the same and correspond to the crystalline silver metal nanoparticles. Yet, the diffraction rings in the inset in Fig. 7f, g, are continuous, unlike the diffraction rings in the insets in Fig. 7h, which are discrete ones. One may conclude that diffraction rings in Fig. 7f, g, are formed as a result of diffraction of electrons on a large number of small nanoparticles, whereas the electron diffraction patterns in Fig. 7h are obtained as a result of electrons diffraction on fewer larger nanoparticles. This correlates well with the direct TEM observations. Indeed, only small silver nanoparticles (clusters) with a size of 1–2 nm were found in films watered from solutions that were at temperatures of 50 °C, 65 °C (Figs. 6, a and b and 7, c and d). In the film obtained from a solution that was at high temperatures of 80 °C and 95 °C, in addition to the phase of small nanoparticles, large AgNPs were also found (Fig. 6, c, d). For a sample obtained from a solution that was at a temperature of 80 °C, the diameter of large particles varied from 10 to 100 nm, the average size of large particles was 25 nm (Table 2). In the film obtained from a solution that was at a temperature of 95 ° C, there are particles of a larger size - from 10 to 150 nm, the average size of large nanoparticles for such a sample is 35 nm.

Comparing the results of XRD and TEM, we can conclude that at high temperatures in solutions of carbonic acid the formation of large AgNPs occurs and this large AgNPs have the structure of polycrystalline metallic silver.

To determine the size of metal nanoparticles, another method was used to study these systems. Weakly concentrated solutions of chitosan with silver nanoparticles were formed in carbonic acid at different temperatures and at a fixed exposure time. These solutions were studied using dynamic light scattering (DLS). It was found that at the temperatures where the precursor solutions for composite films with different structures were obtained, there is a different particle size distribution in slightly concentrated solutions (Fig. 8). For a temperature characterized by the formation of small particles - 50 °C (Fig. 6; Table 2), a distribution with an average particle size increase of about 10 nanometers was revealed (Table 3). As the temperature increases, the average particle size also increases significantly. This

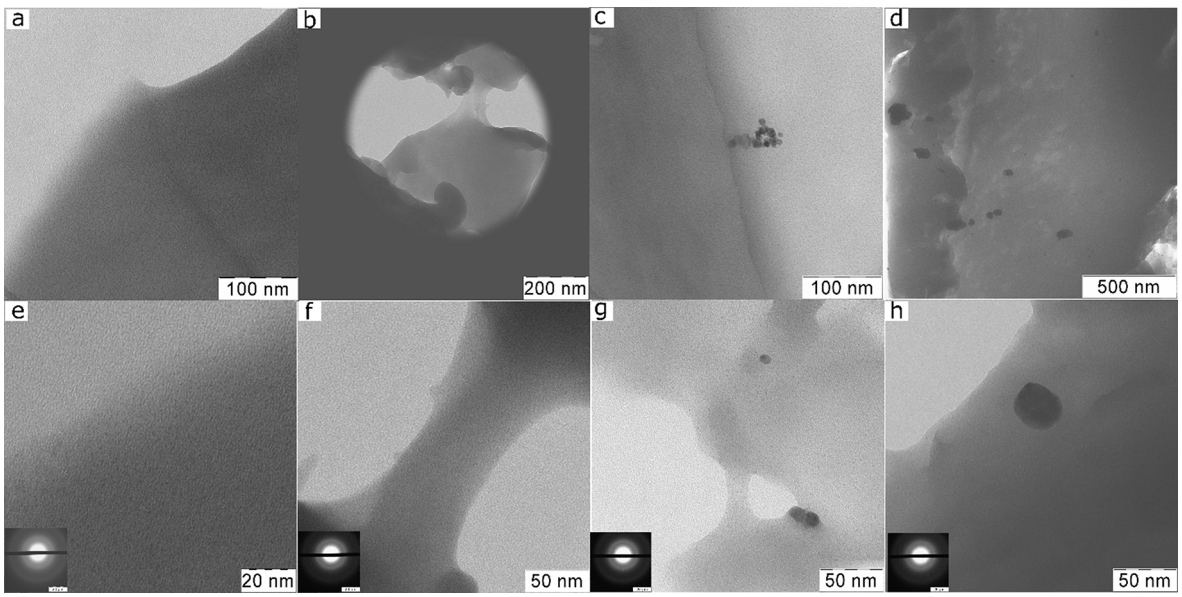

Fig. 6 TEM images of ultrathin sections of composite chitosan films with AgNPs, obtained by irrigation of 1% weight. chitosan solution ($P = 35$ MPa, precursor $AgNO_3$ concentration — 4.5 mM/l, exposure for 8 h at different temperatures: (**a**, **e**) 50 °C; (**b**, **f**) 65 °C; (**c**, **g** 80 °C; (**d**, **h**) 95 °C. Magnification: (**a**, **c**) ×200k, (**b**) - ×100k, (**d**) – ×40k, (**e**) - ×500k, (**f**, **g**, **h**) ×300k. Diffraction patterns for composite films are shown in the lower left corner of the lower row images

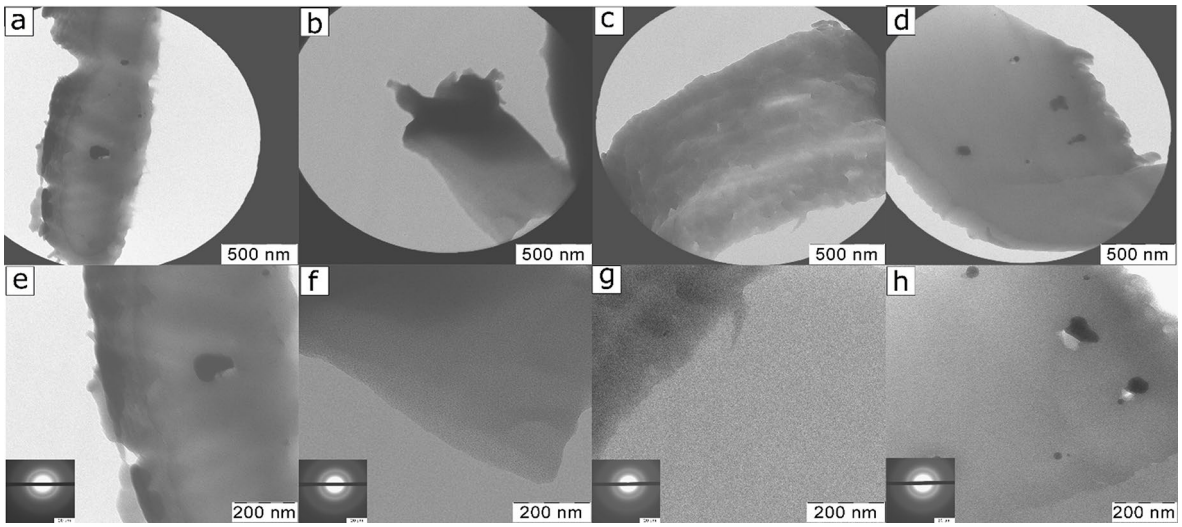

Fig. 7 TEM images of ultrathin sections of composite chitosan films with AgNPs, obtained by irrigation of 1% weight. chitosan solution ($P = 35$ MPa, precursor $AgNO_3$ concentration — 13.5 mM/l, exposure for 8 h at different temperatures: (**a**, **e**) 50 °C; (**b**, **f**) 65 °C; (**c**, **g**) 80 °C; (**d**, **h**) 95 °C. Top row - magnification ×40k (scale line – 500 nm), bottom row - ×100k (scale line – 200 nm). Diffraction patterns for composite films are shown in the lower left corner of the lower row images

Table 2 Comparative analysis of the structure of composite films with AgNPs, obtained from solutions in carbonic acid at P = 35 MPa and with temperature variation (precursor $AgNO_3$ concentration is 4.5 mM/l). The crystallite size is calculated using the full width at half maximum (FWHM) of the (111) reflection, as determined by the Debye-Scherrer equation, for all sample types in Fig. 4

The temperature of the chitosan solution with the precursor Ag NPs	Size of Ag nanocrystals, nm	The average size of AgNPs (M ± m, $n = 100$)	The presence of large AgNPs (> 10 nm, M ± m, $n = 30$)
25	10.0 ± 2.0	9.0 ± 1.0	
50	3.0 ± 1.0	1.5 ± 0.5	Absent
60	3.0 ± 1.0	1.5 ± 0.5	Absent
80	6.0 ± 2.0	4.5 ± 0.5	25 ± 5
95	11.0 ± 2.0	8.0 ± 2.0	35 ± 7

result is consistent with the pattern of TEM image analysis,

Table 3 The results of the DLS analysis of weakly concentrated chitosan solutions with nanoparticles synthesized in carbonic acid solutions at a fixed pressure, exposure time and temperature variation

The temperature of the chitosan solution with the precursor Ag NPs	The average size of AgNPs (M ± m)	PDI
50	10 ± 3	0.42
80	18 ± 4	0.30
95	65 ± 10	0.35

considering the overestimation of the actual size of metallic particles due to the DLS analysis. This overestimation is caused by the binding of metal particles to polymer chains, which leads to an overestimation of the average particle size measured in solution compared to the true value for pure metal particles [51].

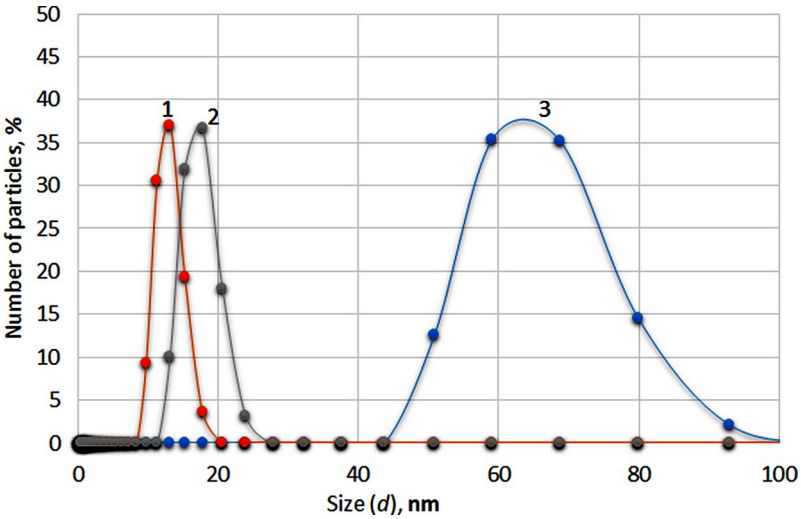

Fig. 8 Size distribution of Ag nanoparticles obtained in chitosan solution (c = 0.5 g/l) in carbonic acid at P_{CO2}=35 MPa, exposure for 8 h at different temperature values: *curve "1"* 50 °C, *curve "2"* 80 °C, *curve "3"* 95 °C. The distributions are obtained by the DLS method

Thus, at a high temperature in a solution of chitosan in carbonic acid not only silver clusters are formed but also clusters are reduced to metal nanoparticles of large size. Indeed, as was recently shown in [42], silver ions in chitosan solutions in carbonic acid are not fully restored. Silver is present in the film in the phase of small particles (clusters), but with further additional reduction by H_2 the particle size increases. Therefore, the temperatures at which the formation of large AgNPs is observed correspond to a more intensive reduction of silver ions in solutions in carbonic acid, which correlates with literature data for composite films obtained from acetic acid [43].

Thus, it was found that forming large AgNPs occur at high temperature, high pressure or high density of CO_2 in the chitosan solution in H_2O/CO_2 biphasic system. Nevertheless, it is possible to identify the following pattern: the structure of films obtained at a pressure of 35 MPa and room temperature (25 ° C) is similar to the structure of films obtained at the same pressure but at a higher temperature — 80 and 95 °C. On the other hand, as for the films obtained at intermediate temperatures of 50 and 65 °C, there is a structure similar to that of films obtained at room temperature, but at lower pressures — 6 and 25 MPa at room temperature [39]. In other words, at a relatively low pressure ($P < 30$ MPa) or at an average temperature of a solution of carbonic acid, the recovery of silver ions by chitosan is less intense than at high pressure and high temperature. Most likely, this pattern is associated with the influence of two factors: the pH of the system, which determines the conformation of the polymer chains, as well as the temperature factor determining the different recovery rates of silver ions, depending on the intensity of thermal motion. Indeed, when the pH is lowered, the polymeric contour is expanded, which increases the reducing ability of chitosan, due to the steric availability of amino and hydroxogroups [52]. With an increase in pH with increasing temperature, the opposite situation occurs — a decrease in the degree of protonability of chitosan polymer chains and, as a result, compaction of the polymer chain. However, as the temperature rises, the reducing ability of chitosan also increases [43], therefore, at a sufficiently high temperature in the carbonic acid, the steric factor is leveled due to the recovery rate of silver ions Table 4.

The antimicrobial properties of composite chitosan films containing both small and large silver nanoparticles were investigated. It was found that films obtained from solutions of chitosan in carbonic acid under different pressures (6, 20, and 35 MPa) had similar antimicrobial properties against all types of pathogenic microorganisms fungi, Gram-positive, and Gram-negative bacteria (Fig. 9). The control pure chitosan film obtained from a solution of chitosan in carbonic acid also has antimicrobial activity, but it is relatively low enough to inhibit pathogens on the surface, which is approximately equal to that of the surface under the sample (Table 4, Fig. 9).The films with both large and small nanoparticles exhibited a significant increase in antibacterial activity against *B. subtilis* ($\Delta I \sim 10 \pm 1\%$, $p < 0.05$, Table 4). In addition, there was a slight increase in activity related to *S. aureus* ($\Delta I \sim 5 \pm 1\%$, $p < 0.05$, Table 4). The more significant impact on Bacillus subtilis bacteria caused by composite films containing both large and small nanoparticles can most likely be attributed to the larger size of these microorganisms compared to other species studied (Table 4) [53]. In the case of larger bacteria, the influence of intense emission of silver ions becomes important, which may occur in the presence of larger metal nanoparticles. Indeed, it is known

Table 4 Analysis of the antimicrobial properties of composite chitosan films with silver nanoparticles obtained by pouring from solutions in carbonic acid under pressure of 60, 200 and 350 atm at room temperature, $AgNO_3$ concentration — 4.5 mM/l, exposure for 8 h. The antimicrobial activity index is calculated according to the ratio presented in Section 2.3.5

#	Reference strain	Composite films obtained by drying chitosan solutions containing Ag NPs that were synthesized in carbonic acid under different pressures.							
		Control (chitosan film without silver nanoparticles)		20 MPa		35 MPa		6 MPa	
1		The diameter of the lysis zone, mm	Antibacterial activity index,%	The diameter of the lysis zone, mm	Antibacterial activity index,%, %	The diameter of the lysis zone, mm	Antibacterial activity index,%	The diameter of the lysis zone, mm	Antibacterial activity index,%, %
1	S.aureus ATCC 29,213	14±1	0	22.0 ± 0.5	36 ± 2	23.0 ± 0.5	40 ± 2	21.0 ± 0.5	33 ± 2
2	Enterococcus faecalis ATCC 29,213	14±1	0	20.0 ± 0.3	30 ± 1	21.0 ± 0.2	33 ± 1	20.0 ± 0.5	33 ± 2
3	Escherichia coli ATCC 25,922	13±1	0	20.0 ± 0.5	35 ± 2	21.5 ± 0.5	40.0 ± 2	20.0 ± 0.5	35 ± 2
4	Pseudomonas aeruginosa ATCC 27,853	14±1	0	21.0 ± 0.2	33.0 ± 1	21.5 ± 0.2	35.0 ± 1	20.0 ± 0.5	33 ± 2
5	Bacillus subtilis ATCC 6630	14±1	0	22.0 ± 0.2	36.0 ± 1	25.5 ± 0.5	45 ± 2	23.0 ± 0.5	40 ± 2

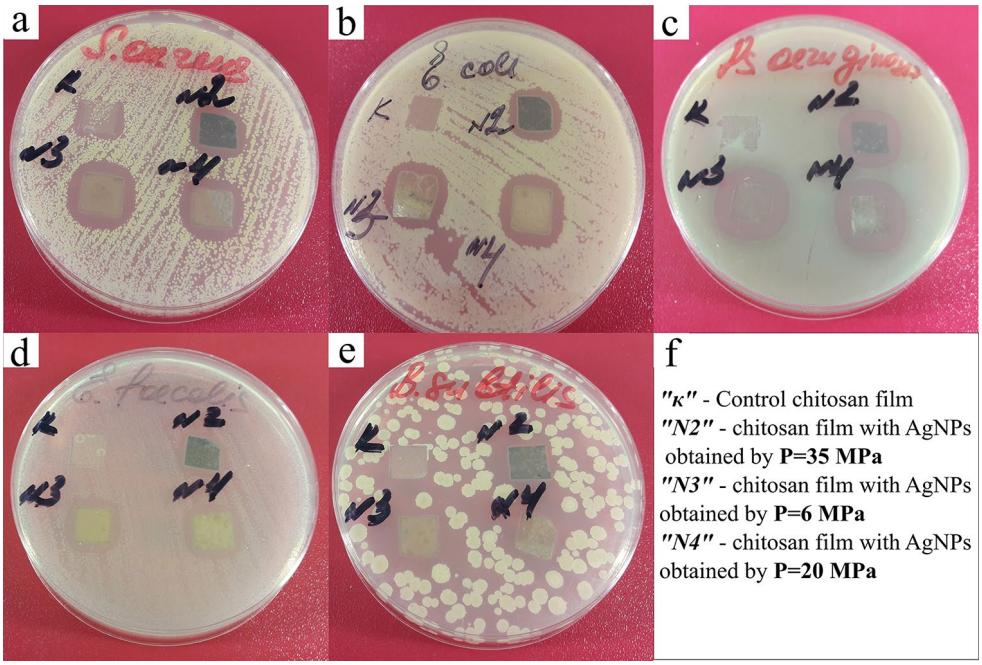

Fig. 9 The results of the antimicrobial test of the composite chitosan films with a structure of both types (only small, both small and large Ag NPs), based on an assessment of the area of the lysis zone of the samples placed on a dense nutrient medium seeded with a lawn of the Museum strains of test-cultures — (**a**) *Staphylococcus aureus ATCC 29,213*, (**b**) *Escherichia coli ATCC 25,922*, (**c**) *Pseudomonas aeruginosa ATCC 27,853*, (**d**) *Enterococcus faecalis ATCC 29,213* and spore-forming culture of (**e**) *Bacillus subtilis ATCC 6630*. The composite chitosan films with (or without for *Control* sample) Ag NPs obtained by drying 1% weight chitosan solution in carbonic acid (T = 25 °C, $AgNO_3$ concentration — 4.5 mm/l, exposure for 8 h at different pressures: 6 MPa, 20 MPa, 35 MPa). The transcription of the film samples is shown in a separate figure (**f**)

that one strategy used by invading microbes is to increase their cell size in order to combat the body's defenses [54–56]. Therefore, it can be assumed that, for the destruction of larger bacteria, a stronger effect from the composite would be effective. This is achieved through the presence of larger nanoparticles with a higher specific ion emission per unit area of contact with the bacterial surface.

4 Conclusion

For the first time, thanks to the combination of various physicochemical methods for studying the structure, it has been demonstrated that it is possible to produce composite chitosan films containing reduced and stabilized silver nanoparticles in carbonic acid solutions under conditions of pressure and temperature variation, and with a relatively short exposure time, without the need for additional chemical reducing agents. It was found that, under certain pressure and temperature conditions, two types of film structure were obtained: one with the presence of only a fine phase of nanoparticles (< 10 nm) and one with the presence of both smaller and larger particles (~ 50–100 nm). It was also found that at relatively low pressures ($P < 30$ MPa) or average temperatures of carbon dioxide solutions, the reduction of silver ions by chitosan occurred less intensely than at higher pressures and temperatures. Most likely, the observed pattern is the result of the combined influence of two factors: the pH of the system, which influences the conformation of the polymer chains, and the temperature, which affects the different rates of extraction of silver ions, depending on the level of thermal motion. Higher antimicrobial activity was observed in composite materials containing both small and large nanoparticles, compared to *B. subtilis*. This may be due to the increased release of silver ions from larger nanoparticles. We believe that the patterns of formation of chitosan composite films revealed in this study could help in the development of new, fully biocompatible composite materials with prolonged antimicrobial activity.

Author Contributions Ivan S. Chaschin, Evgenii I. Perepelkin, Olga A. Kizas, Natalia P. Bakuleva wrote the main manuscript text, Eduard E. Levin prepared Figs. 3 and 4, Sergey S. Abramchuk prepared Figs. 1, 2, 6 and 7, Yulia V. Ryzhova prepared Fig. 8; Table 3, Nelli M. Anuchina prepared Fig. 9; Table 4. All authors reviewed the manuscript.

Funding This work was supported by the Ministry of Science and Higher Education of the Russian Federation (Contract No. 075-00277-24-00).

Data Availability No datasets were generated or analysed during the current study.

Declarations

Competing Interests The authors declare no competing interests.

References

1. S. Prasanna, D. Selvakumar, K. Kadirvelu, N. Kumar, Int. J. Biol. Macromol. (2020). https://doi.org/10.1016/j.ijbiomac.2019.10.113
2. I. Aranaz, A.R. Alcántara, M.C. Civera, C. Arias, B. Elorza, A.H. Caballero, N. Acosta, Polymers (2021). https://doi.org/10.3390/polym13193256
3. C.L. Gîjiu, R. Isopescu, D. Dinculescu, M. Memecică, M.-R. Apetroaei, M. Anton, V. Schröder, I. Rău, Polymers (2022). https://doi.org/10.3390/polym14214492
4. R.R. Almeida, N.A.R. Pinto, I.C. Soares, L.B.C. Ferreira, L.L. Lima, A.A. Leitão, L G L Guimarães Carbohydr. Res. (2023). https://doi.org/10.1016/j.carres.2023.108762
5. S.G. Kou, L. Peters, M. Mucalo, Carbohydr. Polym. (2022). https://doi.org/10.1016/j.carbpol.2022.119132
6. M. Azmana, S. Mahmood, A.R. Hilles, A. Rahman, M.A.B. Arifin, S. Ahmed, Int. J. Biol. Macromol. (2021). https://doi.org/10.1016/j.ijbiomac.2021.07.023
7. Y. Zhao, X. Peng, X. Xu, M. Wu, F. Sun, Q. Xin, H. Zhang, L. Zuo, Y. Cao, Y. Xia, J. Luo, C. Ding, J. Li, Carbohydr. Polym. (2023). https://doi.org/10.1016/j.carbpol.2022.120264
8. S. Shim, H.S. Yoo, Mar. Drugs. (2020). https://doi.org/10.3390/md18120605
9. R. Gobi, R.S. Babu, Mater. Today Commun. (2023). https://doi.org/10.1016/j.mtcomm.2022.105154
10. X. Li, L. Hetjens, N. Wolter, H. Li, X. Shi, A. Pich, J. Adv. Res. (2023). https://doi.org/10.1016/j.jare.2022.02.014
11. C.R. Allan, L.A. Hadwiger, Exp. Mycol. (1979). https://doi.org/10.1016/S0147-5975(79)80054-7
12. D.F. Kendra, L.A. Hadwiger, Exp. Mycol. (1984). https://doi.org/10.1016/0147-5975(84)90013-6
13. P.S. Umoren, D. Kavaz, A. Nzila, S.S. Sankaran, S.A. Umoren, Polymers, (2022). https://doi.org/10.3390/polym14091832
14. A.M. Shehabeldine, S.S. Salem, O.M. Ali, K.A. Abd-Elsalam, F.M. Elkady, A.H. Hashem, J. Fungi, (2022). https://doi.org/10.3390/jof8060612
15. A.H. Hashem, A.M. Shehabeldine, O.M. Ali, S.S. Salem, Polymers (2022). https://doi.org/10.3390/polym14112293
16. E.I. Hassanen, E. Ragab, Biol. Trace Elem. Res. (2021). https://doi.org/10.1007/s12011-020-02143-6
17. M.A. Polinarski, A.L.B. Beal, F.E.B. Silva, J. Bernardi-Wenzel, G.R.M. Burin, G.I.B. deMuniz, H.J. Alves, Part. Part. Syst. Charact. (2021). https://doi.org/10.1002/ppsc.202100009
18. E. Mirda, R. Idroes, K. Khairan, T.E. Tallei, M. Ramli, N. Earlia, A. Maulana, G.M. Idroes, M. Muslem, Z. Jalil, Polymers (2021). https://doi.org/10.3390/polym13223990
19. G.L. Vanti, S. Masaphy, M. Kurjogi, S. Chakrasali, V.B. Nargund, Int. J. Biol. Macromol. (2020). https://doi.org/10.1016/j.ijbiomac.2019.11.179
20. E. Sánchez-López, D. Gomes, G. Esteruelas, L. Bonilla, A.L. Lopez-Machado, R. Galindo, A. Cano, M. Espina, M. Ettcheto, A. Camins, A.M. Silva, A. Durazzo, A. Santini, M.L. Garcia, E.B. Souto, Nanomaterials (2020). https://doi.org/10.3390/nano10020292
21. P. Zhou, Z. Xia, C. Qi, M. He, T. Yu, L. Shi, Int. J. Biol. Macromol. (2021). https://doi.org/10.1016/j.ijbiomac.2021.10.011
22. H. Ye, J. Cheng, K. Yu, Int. J. Biol. Macromol. (2019). https://doi.org/10.1016/j.ijbiomac.2018.10.056
23. E.A. Kukushkina, S.I. Hossain, M.C. Sportelli, N. Ditaranto, R.A. Picca, N. Cioffi, Nanomaterials (2021). https://doi.org/10.3390/nano11071687
24. M. Zienkiewicz-Strzałka, A. Deryło-Marczewska, Int. J. Mol. Sci. (2020). https://doi.org/10.3390/ijms21249388
25. T. Bruna, F. Maldonado-Bravo, P. Jara, N. Caro, Int. J. Mol. Sci. (2021). https://doi.org/10.3390/ijms22137202
26. A. Hamad, K.S. Khashan, A. Hadi, J. Inorg, Organomet. Polym. Mater. (2020). https://doi.org/10.1007/s10904-020-01744-x
27. W. Qian, D. Wei, C. Surf, B. (2008). https://doi.org/10.1016/j.colsurfb.2007.09.030
28. J. Wongpreecha, D. Polpanich, T. Suteewong, C. Kaewsaneha, P. Tangboriboonrat, Carbohydr. Polym. (2018). https://doi.org/10.1016/j.carbpol.2018.07.039
29. W.H. Boehncke, H. Gall, Clin. Exp. Allergy. (1996). https://doi.org/10.1111/j.1365-2222.1996.tb00648.x
30. Y. Nakagawa, Y. Sumikawa, T. Nakamura, S. Itami, I. Katayama, T. Aoki, Allergol. Int. (2006). https://doi.org/10.2332/allergolint.55.411
31. M. Sticherling, J. Brasch, Clin. Dermatol. (1999). https://doi.org/10.1016/s0738-081x(99)00027-9
32. M.A. Silva, A.P. Araujo, J. Souza Ferreira, T.G. Kieckbusch, J. Supercrit Fluids. (2016). https://doi.org/10.1016/j.supflu.2015.11.013
33. A. Zambon, F. Michelino, S. Bourdoux, F. Devlieghere, S. Sut, S. Dall'Acqua, A. Rajkovic, S. Spilimbergo, Dry. Technol. (2018). https://doi.org/10.1080/07373937.2018.1433683
34. V. Santos-Rosales, B. Magariños, C. Alvarez-Lorenzo, C.A. García-González, Int. J. Pharm. (2022). https://doi.org/10.1016/j.ijpharm.2021.121362
35. Y. Sakai, K. Hayano, H. Yoshioka, H. Yoshioka, Polym. J. (2001). https://doi.org/10.1295/polymj.33.640
36. K. Otake, T. Shimomura, T. Goto, T. Imura, T. Furuya, S. Yoda, Y. Takebayashi, H. Sakai, M. Abe, Langmuir (2006). https://doi.org/10.1021/la051662a
37. M.O. Gallyamov, I.S. Chaschin, M.A. Khokhlova, T.E. Grigorev, N.P. Bakuleva, I.G. Lyutova, J.E. Kondratenko, G.A. Badun, M.G. Chernysheva, A.R. Khokhlov, Mater. Sci. Eng. C (2014). https://doi.org/10.1016/j.msec.2014.01.017
38. M.O. Gallyamov, I.S. Chaschin, M.V. Bulat, N.P. Bakuleva, G.A. Badun, M.G. Chernysheva, O.I. Kiselyova, A.R. Khokhlov, J. Biomed. Mater. Res. B (2018). https://doi.org/10.1002/jbm.b.33852
39. I.S. Chaschin, G.A. Badun, M.G. Chernysheva, N.P. Bakuleva, Dokl. Phys. Chem. (2017). https://doi.org/10.1134/S001250161702004X
40. I.S. Chashchin, T.E. Grigor'ev, S.S. Abramchuk, Dokl. Chem. (2016). https://doi.org/10.1134/S0012500816080012
41. I.S. Chashchin, S.S. Abramchuk, L.N. Nikitin, Dokl. Phys. Chem. (2017). https://doi.org/10.1134/S0012501617070041
42. I.V. Novikov, M.A. Pigaleva, S.S. Abramchuk, V.S. Molchanov, O.E. Philippova, M.O. Gallyamov, Carbohydr. Polym. (2018). https://doi.org/10.1016/j.carbpol.2018.02.076
43. H.V. Tran, L.D. Tran, C.T. Ba, H.D. Vu, T.N. Nguyen, D.G. Pham, P.X. Nguyen, Colloids Surf. A: Physicochem Eng. Asp. (2010). https://doi.org/10.1016/j.colsurfa.2010.02.007
44. M.A. Pigaleva, I.V. Elmanovich, Y.N. Kononevich, M.O. Gallyamov, A.M. Muzafarov, RSC Adv. (2015). https://doi.org/10.1039/C5RA18469J
45. E. Levin, I. Treninkov, S. Polyakov, J. Appl. Crystallogr. (2011). https://doi.org/10.1107/S0021889811039537
46. W. Liu, Y. Qin, S. Liu, R. Xing, H. Yu, X. Chen, K. Li, P. Li, Carbohydr. Polym. (2017). https://doi.org/10.1016/j.carbpol.2016.12.040
47. J.R. Deschamps, Powder Diffr. (2013). https://doi.org/10.1017/S0885715612000978

48. P. Scherrer, Nachr. Ges. Wiss. Gottingen. Math. -Phys Kl. **2**, 98 (1918)
49. C. Peng, J.P. Crawshaw, G.C. Maitland, J.P. Martin Trusler, D. Vega-Maza, J. Supercrit Fluids. (2013). https://doi.org/10.1016/j.supflu.2013.07.001
50. M. Ider, K. Abderrafi, A. Eddahbi, S. Ouaskit, A. Kassiba, J. Clust Sci. (2017). https://doi.org/10.1007/s10876-016-1080-1
51. I.O. Wulandari, B.E. Pebriatin, V. Valiana, S. Hadisaputra, A.D. Ananto, A. Sabarudin, Materials (2022). https://doi.org/10.3390/ma15134641
52. A.H. Pakiari, Z. Jamshidi, J. Phys. Chem. A (2007). https://doi.org/10.1021/jp070306t
53. S. Baron, *Medical Microbiology*, 4th edn. (Galveston, University of Texas Medical Branch at Galveston, 1996)
54. J.N. Weiser, Curr. Opin. Microbiol. (2013). https://doi.org/10.1016/j.mib.2013.01.001
55. D.J. Horvath, B. Li, T. Casper, S. Partida-Sanchez, D.A. Hunstad, S.J. Hultgren, S.S. Justice, Microbes Infect. (2011). https://doi.org/10.1016/j.micinf.2010.12.004
56. S.S. Justice, A. Harrison, B. Becknell, K.M. Mason, FEMS Microbiol. Lett. (2014). https://doi.org/10.1111/1574-6968.12602